N. Taymourtash, G. Quaranta
Turbulent Airwake Estimation from Helicopter–ship Wind-Tunnel Data
Journal of Aircraft, published online 17/04/2024
doi:10.2514/1.c037526

Turbulent Airwake Estimation from Helicopter-Ship Wind Tunnel Data

Neda Taymourtash *, and Giuseppe Quaranta†
Politecnico di Milano, Milan, Italy.

This paper presents a stochastic approach for modelling the turbulent airwake suitable for real-time simulation of the Helicopter-Ship Dynamic Interface. This approach relies on the measurements of unsteady loads collected during a wind tunnel test campaign with a scaled helicopter operating over the deck of Simple Frigate Shape1. Power Spectral Densities of the measured aerodynamic loads combined with the estimated Frequency Response Functions are utilized to find, through an optimization algorithm, a model of airwake spectra over the range of frequencies which mainly affects the pilot workload during shipboard operations. Then, a set of Auto-Regressive filters are designed for every particular rotor position and wind-over-deck condition, so that when driven by white noise, the spectrum of the output will reproduce those obtained from the optimization. This approach is applied to three different tested wind directions and three rotor positions, by implementing the Auto-Regressive filters into the multibody model of the experimental rotor. Frequency response analysis of the aerodynamic loads demonstrates that the turbulent airwake model obtained from the experimental data can predict the unsteadiness of loads comparable to those measured in the wind tunnel across the bandwidth of interest for pilot activities. The identified airwake models could be applied to a full-scale model to simulate the unsteady loads effectively experienced by the helicopter during a ship landing flight.

Nomenclature

HSDI	=	Helicopter-Ship Dynamic Interface
WOD	=	Wind-Over-Deck
PSD	=	Power Spectral Density
HW	=	Headwind
R30	=	Red wind from 30°
R60	=	Red wind from 60°

*Post-Doc. Researcher, Department of Aerospace Science and Technology.
†Professor, Department of Aerospace Science and Technology.

rms	=	root mean square
T	=	Thrust force (N)
L, M	=	Roll and pitch moments (N/m)
u, v, w	=	Linear speed velocity components (m/s)
P_{TT}	=	PSD of thrust (N^2/Hz)
P_{LL}, P_{MM}	=	PSD of roll and pitch moments (N^2m^2/Hz)
H_{ij}	=	Frequency Response Function between j-th input and i-th output

I. Introduction

The development of a high-fidelity simulation environment for helicopter shipboard operation is of great importance to reduce the cost and failure risks associated with at-sea flight trials. In the 80s, discussing the substantial increase in helicopter operations in conjunction with various types of ships, Healey proposed the simulation approach in support of flight tests [1]. Since then, a significant amount of research has been dedicated to the development and fidelity assessment of Helicopter-Ship Dynamic Interface (HSDI) simulation. Dynamic Interface (DI) simulations are primarily used to investigate the envelope of safe operations, the so-called Ship-Helicopter Operational Limitation (SHOL) which is a unique envelope for each combination of helicopter and ship [2]. Flight testing at sea is both complex and costly, requiring a dedicated ship and days or weeks of trials [3]. Providing a controllable and repeatable virtual test environment, such simulation platforms can be further exploited to find the approaches that require less pilot workload or to design and test new flight control systems, and for pilot training purposes, developing knowledge at a fraction of the cost and time required to perform a flight test campaign [4].

Assessment of the HSDI simulation demonstrated that airwake modeling is one of the crucial elements that strongly affects the overall fidelity [5] of the simulation environment. The airwake turbulence energy is mostly concentrated in the low-frequency range (below 2 Hz) which covers the bandwidth of closed-loop pilot response frequency between 0.2 and 2 Hz[6]. So, the unsteadiness of the flow field directly affects the handling qualities characteristics. Additionally, piloted simulation of SHOL testing using the steady-state airwake data confirmed that the lack of unsteadiness resulted in lower workloads than normally experienced during the flight test [7, 8]. Consequently, to obtain a realistic level of the pilot workload, both steady and turbulent parts of the airwake need to be correctly modelled.

The main challenge involved in airwake modeling is the mutual interaction of the ship's airwake and rotor-induced flow, which can be taken into account via different approaches. The most representative approach to model this mutual interaction is the development of a fully coupled simulation in which the aerodynamic solver and flight dynamics code should be run simultaneously with the communication between the two codes. However, due to the excessive computational cost, currently, this approach cannot support real-time HSDI simulations [9–12]. A more simplified

approach is a one-way coupled simulation which accounts only for the effect of ship airwake on the rotor inflow [6, 8, 13]. In this approach, the airwake of the ship is pre-calculated, using either steady or unsteady Computational Fluid Dynamics (CFD) without considering the presence of the helicopter. This method represents one of the few viable ways to perform pilot-in-the-loop real-time simulations. The ship airwake velocities are incorporated into the flight dynamics code via look-up tables, assuming the superposition of the ship airwake and rotor-induced flow. Based on subjective pilot workload ratings, this approach could reasonably capture the increased workload due to the influence of the ship's airwake, including the effect of unsteadiness. However, the superposition method has shown a low accuracy for cases of close proximity between the helicopter and the structure of the ship [14].

To reduce the computational resources required to perform coupled simulations, stochastic airwake models were developed that are suitable for real-time piloted simulations. These models could be employed based on both simulation data and flight test measurements in terms of rotorcraft response to environmental turbulence. The stochastic filter generation methods used in HSDI simulations are mostly based on the approach introduced in Refs. [15, 16], in which turbulence models were developed to replicate the response of the UH-60 hovering in the turbulent wake of a hangar. To produce a set of expected pilot inputs, the measured aircraft rates were injected as inputs to an inverse dynamic model obtained starting from an identified model of UH-60. Subtracting the expected inputs from the measured aircraft inputs during the flight test results in remnant values that were interpreted essentially as equivalent turbulence inputs. Then, the resultant disturbance was modelled using white-noise-driven shaping filters, similar to Dryden stochastic turbulence spectral models [17]. These filters were designed to generate an equivalent set of controls to the model with spectral properties as close as possible to the extracted disturbance inputs. When these filters were activated, they recreated a set of disturbances to the aircraft representative of the effect of the original unsteady airwake flow field.

This approach was later modified to obtain the equivalent turbulence model of the ship airwake in terms of linear and angular velocities of an external gust that generates the same rotorcraft response when exposed to the time-varying ship airwake [18, 19]. Only airspeed perturbations with a linear distribution over the rotor disk were considered since it can be shown that thrust and rolling and pitching moments, i.e. the most relevant generalized force perturbations generated by a rotor that affect the aircraft flight mechanics, are strongly related to the linear airspeed distribution (see Chapter 3 of [20]).. The stochastic airwake model was derived from the computed rotorcraft response using a one-way coupled HSDI simulation. The spectral properties of the gust components were analyzed, and shaping filters were designed to simulate the gust disturbances when driven by white noise. The filters had a structure similar to that of the von Karman spectra, which are used to represent atmospheric turbulence at higher altitudes and speeds [21], with the coefficients updated using the best fit to have similar spectral characteristics as what is felt by the aircraft when flies through the ship airwake.

A similar approach was taken in Ref.[22] to derive the stochastic filters from the aircraft response and pilot control activities when hovering at a particular position with respect to the ship deck. The transfer functions of the shaping filters were updated to improve the estimation of spectral density functions. This approach was further improved to

identify the filter coefficients using an Auto-Regressive (AR) model. This algorithm was implemented and tested in a real-time simulation for a UH-60 model hovering in the airwake of two different types of ship classes [23]. While this approach is very effective, it requires the necessity to perform full-scale aircraft flight tests to measure the data to identify the models to be used for flight simulation.

The above-mentioned studies were based on the development of gust or control equivalent models to produce the same effect as turbulence on the rotorcraft response. A different scheme was proposed by Goanakar which relies on the perturbation theory to extract the auto-spectral and cross-spectral densities from the baseline data, including both experimental measurements and CFD solution of the velocity field [24, 25]. In this method, auto-correlation and cross-correlation of the longitudinal, lateral and vertical velocity components were represented by separate perturbation series in which the basis functions have the form of von Karman correlation functions [26]. In a more recent study, the velocity measurements from a wind tunnel test campaign were utilized to estimate the parameters of von Karman spectral functions using system identification techniques [27]. The mean velocity field over the deck of a 1/100-scale model of Simple Frigate Shape 2 (SFS2) was measured through Stereoscopic Particle Image Velocimetry (SPIV) and hot wire anemometry. It should be noted that the computation of the frequency spectrum required the time histories of the velocities at each point that were not measured in the experiment. Consequently, only the gains of the filters were identified, while characteristic lengths set equal to the dimensions of the ship superstructure were used to reconstruct *a posteriori* the velocity spatial distribution.

In addition to the application of the stochastic filters to estimate the turbulent airwake of the ship, this approach was also implemented to represent the unsteady loads of the fuselage, measured in the scaled wind tunnel test, directly into the full-scale flight simulator [6]. In the experiments performed at the National Research Council of Canada (NRC), the unsteady fuselage loads including drag, side force and yawing moment were measured in various wind conditions and for different positions of the helicopter over the deck [28]. The Power Spectral Density (PSD) of the measured unsteady loads was used to compute the filter coefficients, based on the least-square fitting of the spectra. In this way, when the white noise is passed through the transfer function of the filter, the resulting output has the correct magnitude and frequency content of the experimental loads. This approach, different from the previous ones, was based on data collected during wind tunnel tests. However, it did not capture the effects of ship airwake–rotor couplings, because the helicopter model was not included in the experiment. Additionally, the lack of time-resolved data that were difficult to acquire in the experimental set-up employed, allowed only a partial identification of the information necessary to set up the turbulence models. Wind tunnel tests cannot easily measure flow fields continuously in three dimensions since measurement techniques are usually limited to points or plane sampling.

In another effort towards the development of high-fidelity HSDI simulation, a series of experiments were performed in the Wind Tunnel of Politecnico di Milano (GVPM) to investigate the effect of ship airwake on both steady and unsteady aerodynamic loads of a scaled helicopter model in various Wind-Over-Deck conditions [29, 30]. The unsteady

aerodynamic loads of the helicopter model were measured while the rotor was trimmed at different positions along a landing trajectory over the deck of a 1/12.5-scale model of Simple Frigate Shape 1 (SFS1). The measured time histories of the aerodynamic loads are being used in the current work to develop the stochastic simulation framework. It should be noted that to accurately reconstruct the turbulent flow field in a fully coupled environment, i.e., a helicopter operating over the deck in windy conditions, an unsteady velocity field should be measured within the landing area. So, a database of the temporal and spatial distribution of the velocity is needed which is extremely challenging to measure in the experiments, especially if the helicopter model is moving in the wind tunnel, for instance in the experiments reported in Ref. [30]. This is the reason why in the previous works where the experimental database has been used to design the stochastic filters [25, 27], the measurements were related to an isolated ship test. On the other hand, aerodynamic loads can be measured by designing a fairly simple setup which consists of a strain gauge balance calibrated for the expected range of frequency and amplitude of the loads in all directions [30]. In this way, when the helicopter is hovering or moving over the flight deck, the aerodynamic loads affected by the mutual interaction of the ship airwake and rotor downwash can be measured with a sufficiently high sampling rate, so that the frequency analysis can be performed over the range of interest for flight mechanics and assessment of handling qualities [31].

The stochastic simulation framework proposed in this research is based on the unsteady load measurements to design the stochastic filters representing the unsteady flow field of a fully coupled environment. The load measurements are combined with the estimated Frequency Response Functions (FRFs), based on validated numerical models of the wind tunnel model dynamics, to obtain the PSDs of the gust perturbations through an optimization algorithm. Then, the AR modeling technique is employed to derive the shaping filters required for the stochastic simulation. Finally, the filters are implemented into the multibody model developed for the experimental rotor and three different WOD conditions are simulated. To evaluate the performance of the designed filters, the unsteady aerodynamic loads obtained from the simulation will be presented and compared with the experimental measurements. The advantage of this approach to what has been previously developed is to demonstrate the possibility of generating stochastic filters for the turbulence applicable to full-scale simulation models, starting from wind tunnel data that takes into account the aerodynamic coupling of the rotor with the ship airwake, however at a fraction of the cost and time of at-sea flight test campaigns. The availability of a rotor in the wind tunnel that develops thrust and aerodynamic moments allows for the creation of the correct aerodynamic induction effect and the consequent establishment of the fully coupled aerodynamic flowfield.

II. Experimental Test

The setup consists of a 4-bladed helicopter with a radius of 48.5 cm and a simplified ship model, representative of the 1:12.5 scale model of Simple Frigate Shape1 (SFS1). The helicopter model was held by a horizontal strut connected to a system of two motorised orthogonal sliding guides which can change the relative position of the helicopter in both vertical and longitudinal directions. A detailed description of the setup, instrumentation and measurements can be

found in [30].

To simulate a typical stern landing trajectory, four points were considered along a descent path with a slope angle of 15° towards the landing point. Three additional points were also selected to be representative of a vertical descent over the deck. At each test point, an initial trim procedure was performed to obtain a specific level of thrust and zero in-plane moments by applying collective and cyclic commands. Then, trim commands were fixed and the acquisition of the loads was performed for 30 seconds with the sampling frequency of 100 Hz and repeated twice for each point. These time histories are used in the current study to design the stochastic filters. Test parameters, including wind speed and rotor rpm were selected based on the similarity of Strouhal number compared to Bo-105 as a generic medium–size full–scale model. A detailed description of the scaling parameters can be found in [30].

It is important to emphasize that to avoid overloading the swashplate mechanism that was not designed specifically for this test, a thrust coefficient of 60% of the full-scale value (see Table 2) has been used since the objective of the experiment was not the ship landing performance of the Bo-105 helicopter, but to verify if the proposed experimental approach is an effective instrument to study the steady and unsteady loading of a rotor operating in a fully-coupled environment [30].

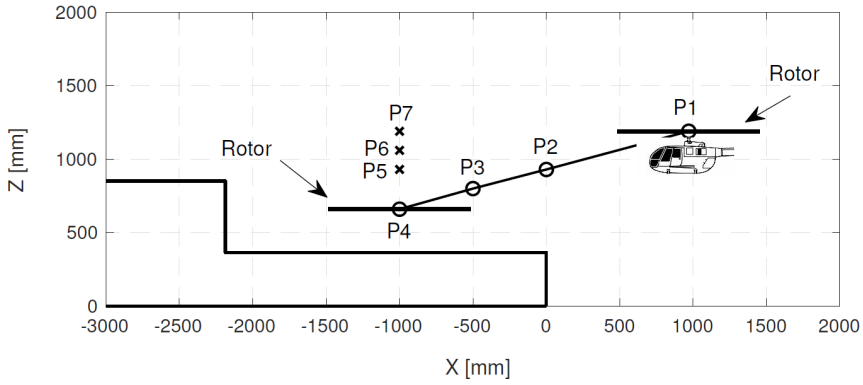

Fig. 1 Side-view of the test points. Circles and crosses represent the position of the rotor center in stern landing and vertical descent, respectively [30].

Here, three rotor positions are selected to present the results of the stochastic simulation. Furthermore, three wind directions are considered at each test point, including headwind (HW), Red Wind from 30° and 60°, where red indicates a wind coming from the port side, with a full-scale velocity of 20 knots in all three directions. Table 1 summarizes the rotor position and wind condition of the test points selected for this work.

III. Numerical Framework

In this section, the numerical framework of the stochastic simulation will be presented. Figure 2 shows the proposed approach, starting from wind tunnel tests towards generating unsteady turbulence effects enable to reproduce the same

Table 1 Rotor position and WOD condition for selected test points.

Test Point	X [mm]	Y [mm]	Z [mm]	WOD
P3	-500	0	800	HW-R30-R60
P4	-1000	0	660	HW-R30-R60
P7	-1000	0	1190	HW-R30-R60

loads measured in the experiment. First, a multibody model of the experimental rotor has been developed (section III.A). Then, a representative CFD solution of the ship airwake must be computed and incorporated into the multibody simulation via the one-way coupling approach (section III.B). The one-way coupled model is used only to trim the rotor loads close to the experimental ones. The multibody model is also used to estimate the FRF of the aerodynamic rotor hub loads due to external gust components at each trim condition (section III.C). Then, a set of optimized stochastic models for different gust speed components can be identified, to obtain the load spectra measured in the experiment, given the FRFs from the previous step (section III.D). The resulting stochastic models for the gust components are implemented into the multibody simulation environment, to model the helicopter-ship aerodynamic interaction.

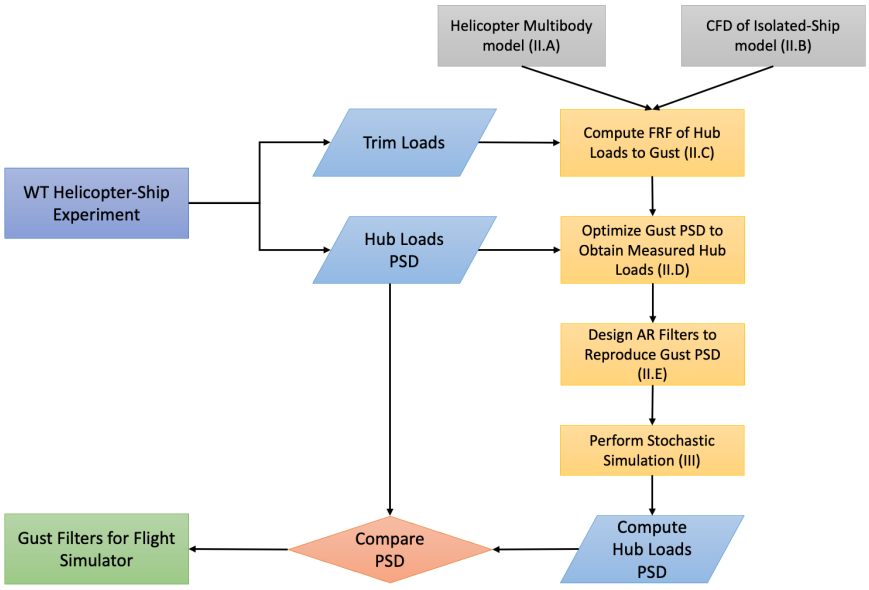

Fig. 2 Flow chart of the process to generate unsteady airwake disturbances on the helicopter.

A. Multibody Model

A multibody model of the experimental rotor has been developed using MBDyn, a free general-purpose multibody dynamics analysis software developed at Politecnico di Milano [32]. MBDyn features the integrated multidisciplinary simulation of multibody systems, including nonlinear mechanics of rigid and flexible bodies subjected to kinematic constraints, along with smart materials, electric and hydraulic networks, active control and essential elements of

rotorcraft aerodynamics [33].

The multibody model developed for this study consists of a hingeless, stiff-in-plane rotor with four elastic blades connected to the hub through a revolute hinge, which allows the rotation around the feathering axis of the blade. This degree of freedom, along with a rigid pitch link connected to the swashplate provides the ability to apply collective and cyclic pitch controls to trim the aerodynamic loads.

It must be noted that at the geometric scale, a stiff-in-plane rotor is the only viable option for a wind tunnel model. Such a system can develop thrust and control moments in similitude with the full-scale system, but the rotor dynamics are expected to be different from the one of the full-scale system. This change can lead to different handling qualities for the full-scale system compared to those of the wind tunnel model (see [20]). Consequently, it should not be considered correct to apply a scaled version of the hub loads measured on the wind tunnel model — that can be identified through the approach presented in [30] — to the full-scale model, but it is instead necessary to identify the flow perturbations that cause these loads and then apply these perturbations to the full-scale model that, in the flight simulation environment, will react to them with the correct dynamics.

Each blade is modelled by three finite volume beam elements composed of three nodes (see Ref. [34]) so that the constitutive properties of each section can be defined separately. To introduce the aerodynamic model, *Aerodynamic Beam* element is implemented which relies on the structural beam element to compute the configuration of the aerodynamic surface at each integration point. Aerodynamic loads are computed based on Blade Element/Momentum Theory, using c81 aerodynamic table of NACA0012 defined as the airfoil of the blades. The inflow of the rotor is represented by the Pitt-Peters dynamic inflow model [35] with three states, including uniform and linear perturbations of the wake-induced downwash at the rotor disk. The parameters of the model are selected the same as the parameters of the experimental rotor introduced in [30]. Selection of the test parameters in that experiment led to a geometric scale of 1:10.1, velocity scale of 1:2.1 and frequency scale of 4.75:1. All these three scaling factors are maintained in the simulations performed in the current study.

Table 2 Parameters of the experimental helicopter model and Bo105 as full-scale reference aircraft.

Characteristic	Scaled Model	Bo105
Number of Blades	4	4
Rotor Radius (m)	0.485	4.91
Angular Speed (rad/s)	211	44.4
Blade Chord (m)	0.042	0.27
Free Stream Velocity (m/s)	4.8	10.3
Advance Ratio	0.047	0.047
Tip Mach Number	0.3	0.63
Tip Reynolds Number	$2.9e5$	$3.9e6$
Thrust Coefficient	0.0028	0.0046

B. Airwake Coupling

To incorporate the airwake of the ship into the numerical model of the rotor, the one-way coupling approach is implemented. In this approach, the airwake of the isolated ship has been pre-calculated using a steady or unsteady CFD simulation and will be incorporated into the flight dynamics code via look-up tables.

Here, the results of time-accurate CFD simulations performed for the full-scale SFS2 geometry are implemented in the multibody simulation, providing a three-dimensional time-varying velocity field over a region of interest around the deck. The time-varying airwake velocities were stored every 0.05 seconds for a total time of 30 seconds. The SFS2 is an updated version of the SFS1 with a more elongated superstructure and pointed bow. The topology of the flow over the deck is similar for both cases as reported in [36–38]. The differences are mainly concentrated on the turbulent components of the flow. However, the data of CFD simulation of the SFS2 are used only to trim the multibody model, so the impact of the geometrical differences is expected to be limited.

Since the flow field can be considered independent to the Reynolds number, the simulations were performed with an inlet velocity of 40 knots, but can be scaled for other wind speeds. Details of the computational approach and validation of the model can be found in [39]. To implement the database in the multibody simulation, the size of the domain and the airwake velocities are scaled using the geometry and velocity scales of the experimental test, introduced in Table 2.

To apply the effect of the airwake velocity on the aerodynamic elements of the rotor, a 3-dimensional interpolation is performed at every time step and for each aerodynamic integration point. Regarding the spatial and temporal distribution of the airwake data, each aerodynamic element of the rotor blades will experience a local velocity vector depending on its position within the grid. Then, the local aerodynamic forces and moments are integrated along the spanwise direction of each blade and transferred into a non-rotating reference frame, with the origin on the centre of the hub, x-axis from nose to tail, z-axis from bottom to top and y-axis towards the starboard. The aerodynamic loads in the following section will be presented in this reference, referred to as the "rotor reference frame".

A trimming procedure is performed in which a feedback controller is employed to obtain the collective and cyclic controls required to trim the aerodynamic loads of the rotor while it is subjected to the unsteady airwake of the ship. The objective of the trim is defined the same as the experiment: to maintain a constant thrust coefficient and zero in-plane moments so that the tip-path plane remains parallel with respect to the relative wind. Then, to proceed with the stochastic simulation, the time-averaged controls obtained from the trimming procedure are maintained, while the unsteady CFD database is replaced by the time-averaged data. Consequently, it can be ensured that the trim condition is respected in all test points, and the additional unsteadiness due to the mutual interaction of the rotor inflow and ship airwake will be added by implementing the stochastic filters.

Figure 3 shows an example of the contours of time-averaged normalized velocity magnitude at the rotor height while placed at the position with the lower altitude (Z = 660 mm) shown in Fig. 1, with the wind blowing from three different directions.

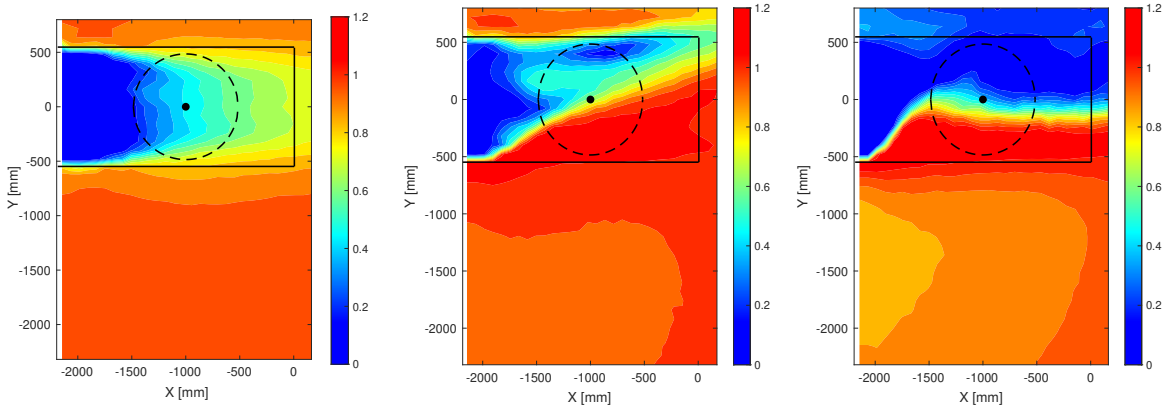

(a) HW (b) R30 (c) R60

Fig. 3 Contours of time-averaged non-dimensional airwake velocity magnitude ($|\bar{U}|/U_\infty$) at P4 (Z = 660 mm).

C. Frequency Response Function Estimation

The FRFs are estimated using the input-output data collected from the numerical simulation at each test point. The FRFs are transfer functions representing the aerodynamic response of the rotor while being excited by an external gust velocity vector. These FRFs could present a dependency on the exact trim condition, which in turn may be slightly different if a one-way or two-way coupled flow-field is considered. However, taking into consideration that the rotor is trimmed at the same average loads measured in the tests and that a linear aerodynamic behaviour of the blades can be considered for small perturbations due to turbulence, the dependency is expected to be negligible. FRF estimation has been performed considering a Multi-Input Multi-Output (MIMO) system with three components of the gust velocity (vertical, longitudinal and lateral), constant in space for the entire rotor disk, as the excitation input and three aerodynamic loads of the rotor (thrust, roll and pitch moments) as the output of the system.

The excitation inputs are designed based on orthogonal multi-sine signals with optimized phase shifts. In this method, each input is a sum of harmonic signals with a unique set of discrete frequencies which are selected to cover the whole bandwidth of interest [40]:

$$u_i = \sum_{k=1}^{M} a_k \sin(\omega_k t + \phi_k) \tag{1}$$

where M is the total number of discrete frequencies within the range of interest. To cover the whole bandwidth for each input, while satisfying the mutual orthogonality, the frequencies are interleaved among three inputs in an alternating manner. Consequently, the mutual orthogonality of the excitation signals is guaranteed in both time and frequency domains.

As mentioned before, the relevant range of frequency for unsteady load analysis in full scale is up to 2 Hz. Considering the frequency scale of 1:4.75, introduced in the previous section, the bandwidth of interest corresponds to the range of $[0.95 - 9.5]$ Hz at the scale of the model. The FRF estimation should be performed across this bandwidth.

Consequently, the range of $[0.2 - 10.2]$Hz is discretized with the resolution of 0.2 Hz which results in a total of 51 harmonics, i.e. 17 distinct harmonics for each input signal.

In general, the combination of sinusoids with different harmonics may result in relatively large peaks which is not desirable, since it can drive the system too far from the reference trim condition. To avoid this issue, the phase shift can be found via an optimization algorithm to minimize the Relative Peak Factor (RPF), defined as [41]:

$$RPF(u_i) = \frac{\max(u_i) - \min(u_i)}{(2\sqrt{2})\text{rms}(u_i)} \tag{2}$$

Alternatively, an analytical solution was proposed by Schroeder [42] which results in a relatively low peak factor and reduces the computational costs, especially for cases with a large number of optimization variables. In this work, Schroeder formulation is used which reduces to the following distribution of phase shifts ϕ_i to obtain a power that is uniformly distributed between all harmonics of the multi-sine signal [42]:

$$\phi_k = \phi_1 - \frac{\pi k^2}{N} \quad k = 1, 2.., N \tag{3}$$

where $N = 17$ is the total number of harmonics for each input. Finally, the amplitude of individual harmonics can be selected independently to obtain a specific power distribution. Here, a uniform distribution is considered, with a which should be selected small enough to avoid the appearance of significant nonlinear effects in the output loads.

$$a_k = \frac{a}{\sqrt{N}} \tag{4}$$

In the next step, three multi-sine inputs representing longitudinal, lateral and vertical airspeed perturbations are applied to the model. In each simulation, the perturbations are superimposed to the WOD condition, where the same trim condition as the experiment is maintained by using the mean collective and cyclic commands identified during the previous trimming procedure. Both input and output time histories are transformed into the frequency domain using the finite-time Fourier transform. Since the inputs are uncorrelated, the estimate of the FRF between each pair of input-output can be obtained as follows:

$$H_{ij}(f_k) = \frac{Y_i(f_k)}{X_j(f_k)} \tag{5}$$

where Y_i and X_j are Fourier transforms of the output (thrust, roll or pitch moment) and input (vertical, longitudinal or lateral perturbation velocity), respectively. At each test condition, three inputs are applied to the system simultaneously, and the aerodynamic loads are recorded as the output signals. Consequently, at each discrete frequency the input-output

relationship, with uncorrelated inputs, can be represented through the following matrix form:

$$\begin{Bmatrix} P_{TT}(\omega_i) \\ P_{LL}(\omega_i) \\ P_{MM}(\omega_i) \end{Bmatrix} = \begin{bmatrix} |H_{Tw}(\omega_i)|^2 & |H_{Tv}(\omega_i)|^2 & |H_{Tu}(\omega_i)|^2 \\ |H_{Lw}(\omega_i)|^2 & |H_{Lv}(\omega_i)|^2 & |H_{Lu}(\omega_i)|^2 \\ |H_{Mw}(\omega_i)|^2 & |H_{Mv}(\omega_i)|^2 & |H_{Mu}(\omega_i)|^2 \end{bmatrix} \begin{Bmatrix} P_{ww}(\omega_i) \\ P_{vv}(\omega_i) \\ P_{uu}(\omega_i) \end{Bmatrix} \tag{6}$$

where P_{ii} represents the PSD of each signal.

Figure 4 shows the estimation of FRFs obtained for the trimmed rotor at P4 in the headwind condition. It can be seen that there is one dominant response for each aerodynamic load, which corresponds to the diagonal terms in the FRF matrix (Eq. 6). As expected, the thrust is affected mainly by the vertical gust due to the change in the mean induced flow over the rotor disk area. Lateral and longitudinal gust perturbations modify the lateral and longitudinal distribution of the inflow and consequently affect the roll and pitch moments, respectively. However, the off-diagonal terms also should be estimated, as their relevance may change depending on the reference wind condition. For instance, in the headwind condition as represented in Fig. 4, the effect of the longitudinal gust speed on thrust is the secondary effect and the lateral gust is almost ineffective. However, when testing with large wind angles, like R60, the effect of lateral and longitudinal disturbances is reversed.

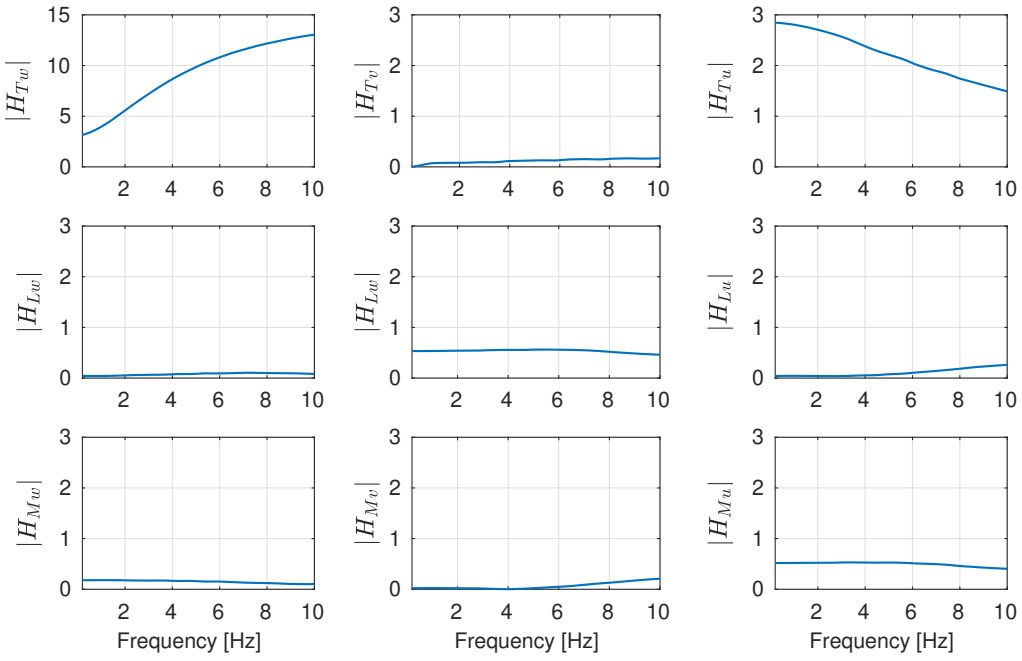

Fig. 4 Estimated FRFs in HW test condition with the rotor at P4.

D. Estimation of the Airspeed Perturbation

Assuming that the same input-output correlation applies to the experimental model, the estimated transfer functions can be employed to obtain the PSD of the gust disturbances, as the unknown input, so that the output will be the best fit to the PSD of the measured loads. So, the system of linear equations, represented in Eq. 6, could be solved at all discrete frequencies. Regarding the differences between the numerical and experimental models, a constrained optimization problem is defined to minimize the summation of the relative error from three equations:

$$e = \sum_{j \in (T,L,M)} \frac{\left| P_{jj_{\text{exp}}} - \sum_{i \in (w,v,u)} H_{ji}^2 P_{ii} \right|}{P_{jj_{\text{exp}}}} \tag{7}$$

Since the optimization variables are the power of the gust disturbances at each discrete frequency, they must remain positive over the range of interest. It should be noted that the defined cost function consists of three equally important terms. So, each term is only normalized with respect to its reference value to avoid having terms with different sizes. If needed, weighting factors can be considered for each term to improve the quality of the solution for certain coefficients, according to the additional requirements of a specific problem. The optimization problem has been solved using the *fmincon* routine in MATLAB utilizing the interior-point algorithm [43]. The PSDs obtained from the optimization are then transformed back to the time domain using the inverse of the Fourier transform. These time histories are employed to design the stochastic filters with the AR modelling technique which is discussed in the following section.

E. Auto-Regressive Filter Design

AR model is a linear predictive modelling technique that estimates the variable of interest using a linear combination of the past values of the variable. If $y(n)$ is the current value of the variable of interest, then an AR model of order p can be written as:

$$y(t) + \sum_{k=1}^{p} a(k) y(t-k) = w(t) \tag{8}$$

where $a(k)$ is the auto-regression coefficients and $w(t)$ is a zero-mean white noise. Converting the signal into the frequency domain, using the z-transform, the Eq.8 can be rewritten as:

$$y(t) = \frac{w(t)}{1 + \sum_{k=1}^{p} a(k) z^{-k}} = \frac{w(t)}{A(z)} \tag{9}$$

where z^{-1} is the unit delay operator ($z^{-k} y(t) = y(t-k)$) and $A(z)$ is a polynomial function composed by the auto-regression coefficients to be identified. By assumption, $y(t)$ is a finite series and so $A(z)$ cannot have any zeros exactly on the unit circle. Furthermore, it is always possible to choose $A(z)$ so that all poles are inside the unit circle. Consequently, the asymptotic stability of the estimated AR model can be guaranteed [44]. PSD of the rational transfer function of Eq.9, which depends on the frequencies of the random process (ω), the variance of the white noise (σ_p^2) and

auto-regression coefficients (a_k), can be computed as the following equation [45]:

$$S(\omega, a_k, \sigma_p^2) = \frac{\sigma_p^2 \Delta t}{\left|1 + \sum_{k=1}^{p} a(k) e^{-2\pi j f k \Delta t}\right|^2} \tag{10}$$

where Δt is the sampling period and $f < f_N$ with f_N the Nyquist frequency). The auto-regression coefficients characterize the PSD of the time series. Consequently, finding the best values for $a(k)$ coefficients gives the best PSD estimation of a random process ($y(t)$) represented by an AR model.

As seen in the above equations (10), an advantage of the AR modelling technique, as one of the parametric methods, is that it operates on time-domain data to find the best PSD estimation. Furthermore, the estimation of parameters in AR model is a well-established topic based on solving a system of linear equations, with several techniques developed to improve the accuracy and computational efficiency. Consequently, the AR modelling technique can be potentially implemented in the real-time estimation of the stochastic filters, which could be of interest for the future developments of this study. This error is defined as the difference between the total power of the gust spectra obtained through optimization (see section III.D) and the output of AR filters, both computed over the frequency range of interest. After performing multiple simulations at each test point to identify the minimal model order sufficient to bring the error below the selected threshold, a third-order AR model was found to satisfy this criterion in all test conditions. Figure 5 compares the PSDs obtained through the optimization and the output of the AR filters of order three, driven by white noise. The AR filters can reconstruct the spectral properties of the gust perturbations with an acceptable level of approximation over the whole range of frequencies. This has been verified for all test conditions so that it has been possible to define a set of filter coefficients to be implemented in the stochastic simulation.

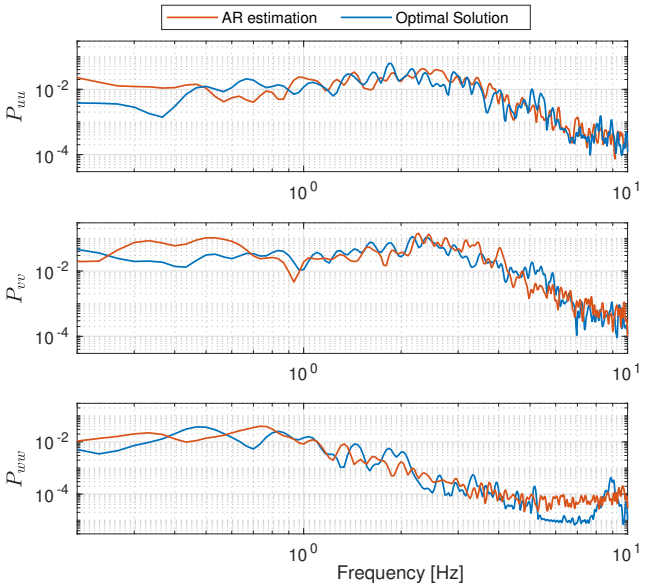

Fig. 5 PSD of gust disturbances in HW with the rotor at P4.

IV. Stochastic Simulation

To evaluate the effectiveness of the stochastic airwake modeling, the simulation results will be presented and compared against the experimental measurements. It should be mentioned that to represent the deterministic part of the airwake, the mean velocity field obtained from the solution of time-accurate CFD is implemented in the multibody model via the one-way coupling approach, explained in section III.B. The stochastic part, which accounts for the unsteady effects of the airwake, is generated through the AR filters driven by white noise, representing three components of the gust disturbances applied to the model. Furthermore, to maintain the trim condition similar to the experiment, the time-averaged collective and cyclic controls obtained from the trimming procedure are applied during the 30 seconds of the stochastic simulation. Consequently, the steady aerodynamic loads remain similar to the experiment, while the unsteady part can be evaluated by comparing the PSDs across the low-frequency bandwidth.

Figure 6 compares the PSDs of the aerodynamic loads, including thrust, roll and pitch moments from the simulation and experiment for three different rotor positions in HW. First, it can be seen that the overall trend of the spectrum across the bandwidth is very well captured by the stochastic simulation. Both experimental and simulation results indicate that the load spectra are relatively constant in the lower frequencies and tend to decrease from 2-3 Hz up to 10 Hz. Furthermore, Fig. 6 shows that in all three rotor positions, while the unsteadiness of the thrust and roll moment is

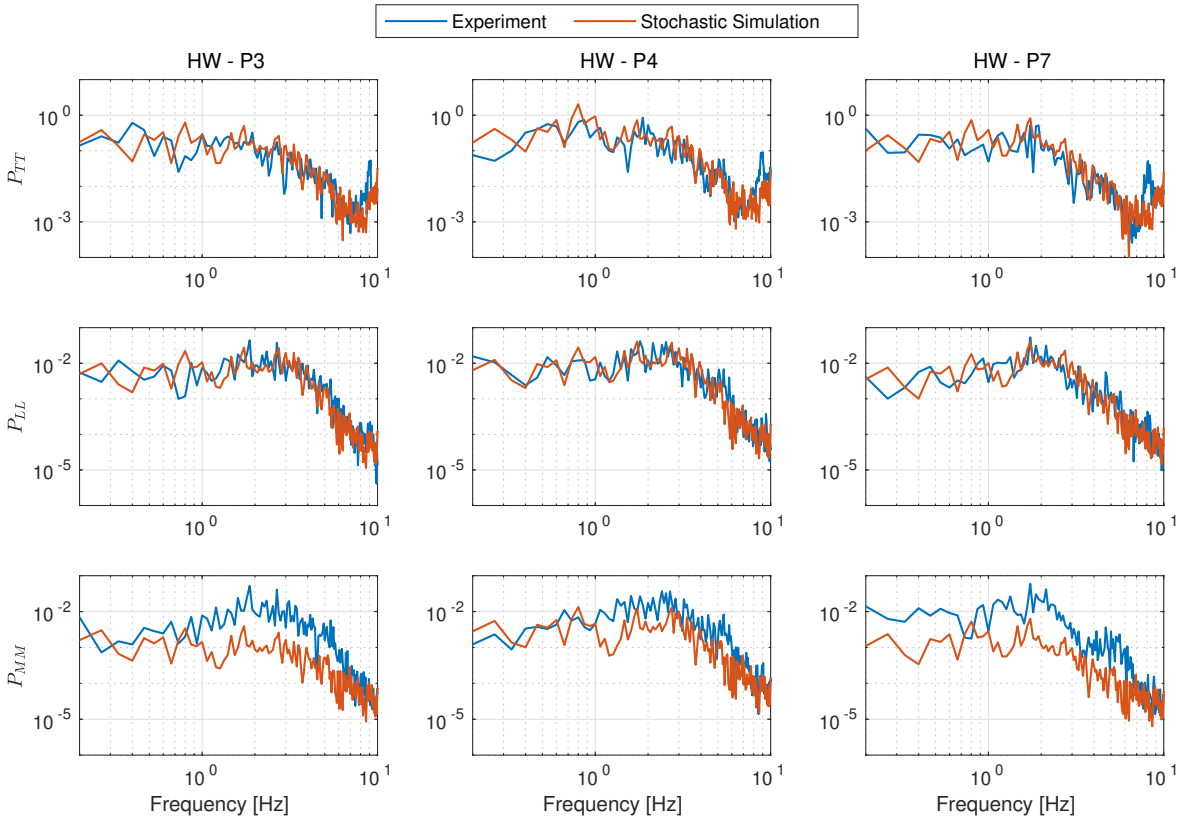

Fig. 6 PSD of the aerodynamic loads in HW test condition.

well predicted, the unsteadiness of the pitch moment is underestimated in the simulation. Looking at the estimated FRFs in HW, presented in Fig. 4, it can be seen that lateral gust perturbation mainly affects the roll moment and its effect on the thrust and pitch moment are almost negligible. On the other hand, the longitudinal perturbation affects both the pitch moment and thrust. Therefore, the lateral gust will be used as an almost independent variable in the minimization problem (defined in Eq. 7) to find the best fit for the PSD of the roll moment. Then, the other two variables, vertical and longitudinal perturbations, were identified imposing the minimization of the total error. Regarding the higher sensitivity of the thrust concerning the vertical and longitudinal perturbations (refer to Fig. 4) the optimization procedure tends to decrease the error of the thrust more than the pitch moment. Consequently, when the AR filters designed based on the optimal solution are employed to perform the stochastic simulation, more discrepancies are observed in the PSDs of the pitch moment compared to those of the thrust and roll moment. Further stochastic models can be derived in any intermediate spatial position by applying appropriate interpolation procedures to the identified AR filters. However, this extension has not been pursued in this work.

As listed in Table 1, the stochastic simulation has been performed in two other WOD conditions, including R30 and R60. Figures 7 and 8 present the PSDs of the aerodynamic loads in R30 and R60, respectively. Overall, it can be seen that the AR filters can predict unsteady loads with non-zero wind angles and different rotor positions over the deck. In the R30 test condition, similar to the HW, the roll moment shows the most accurate results and the main difference with respect to the experimental data is related to the pitch moment.

It is expected that with large wind angles, the effect of the lateral and longitudinal gust perturbations on the thrust will be reversed. Consequently, in R60 test condition, the thrust will be more sensitive to the perturbation of the lateral gust than the longitudinal one. This is the reason why in R60 the spectrum of the pitch moment has been predicted accurately, while the PSD of the roll moment shows more deviation concerning the experimental results.

The presented results confirm that the stochastic simulation can reproduce the experimental spectra in various WOD conditions. These low-frequency perturbations, which are the results of the mutual interaction between the rotor inflow and ship airwake, should be counteracted by the pilot. So, it can be expected that by correctly replicating the unsteadiness, a realistic level of pilot workload will be obtained in the piloted simulation of HSDI. As a matter of fact, performing the piloted simulation is necessary to evaluate the effect of thrust, roll and pitch unsteadiness on the pilot workload and to quantify an acceptable tolerance for the prediction of each load component. This evaluation would be beneficial to set the weighting factors in the cost function. In this way, instead of having three equally important terms, the prediction of the load component which was found more critical for the pilot can be improved.

V. Conclusions

In this study, a stochastic airwake modeling approach has been proposed to be implemented in the real-time HSDI simulation. This approach relies on the experimental data collected in a wind tunnel test campaign that was performed

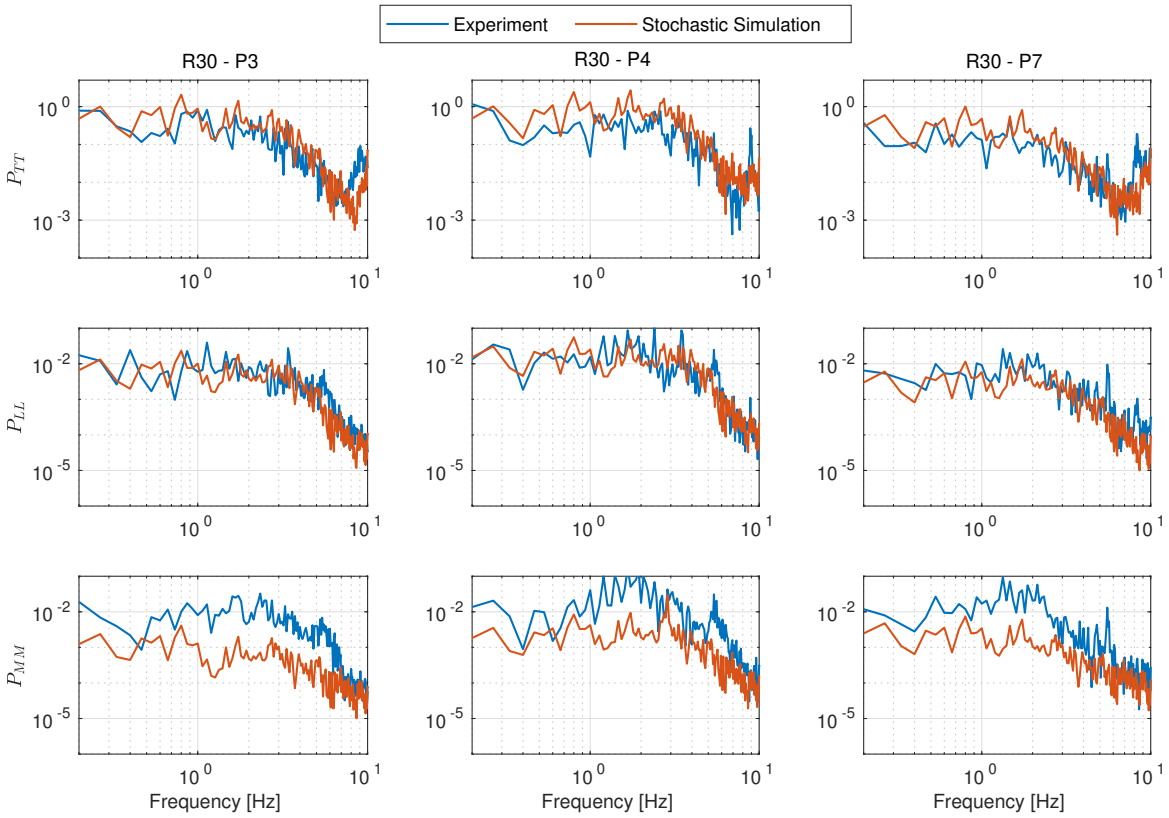

Fig. 7 PSD of the aerodynamic loads in the R30 test condition.

to study the unsteady loading of a scaled helicopter model operating over the deck of SFS1 in various WOD conditions.

A numerical model of the experimental rotor has been developed to simulate the same test condition as the experiment. In the first step, the time-accurate CFD solution of the isolated-ship airwake has been implemented via the one-way coupling approach. The coupled simulation has been used to obtain the required collective and cyclic controls to maintain the trim condition at each test point similar to the experiment. Then, the trimmed model was utilized to identify FRFs representing the variation of the aerodynamic loads due to an external gust element including vertical, longitudinal and lateral perturbations. The FRFs were identified at discrete frequencies covering the whole range of interest for the pilot activities, equivalent to 0.2 up to 2 Hz in the full-scale model. The identified transfer functions were combined with the experimental spectra of the aerodynamic loads to obtain the frequency spectrum of the three components of the gust perturbations through an optimization algorithm. These spectra which are representative of the low-frequency turbulent airwake were used to design the AR filters for each specific test point. When these filters are driven by a zero-mean white noise, the spectrum of the output will be similar to those obtained from the optimization. Consequently, it can be expected that by implementing these filters into the simulation, the unsteady aerodynamic loads will have similar spectra to those measured in the wind tunnel test.

To evaluate the proposed approach, the stochastic simulation was performed in three wind directions, including

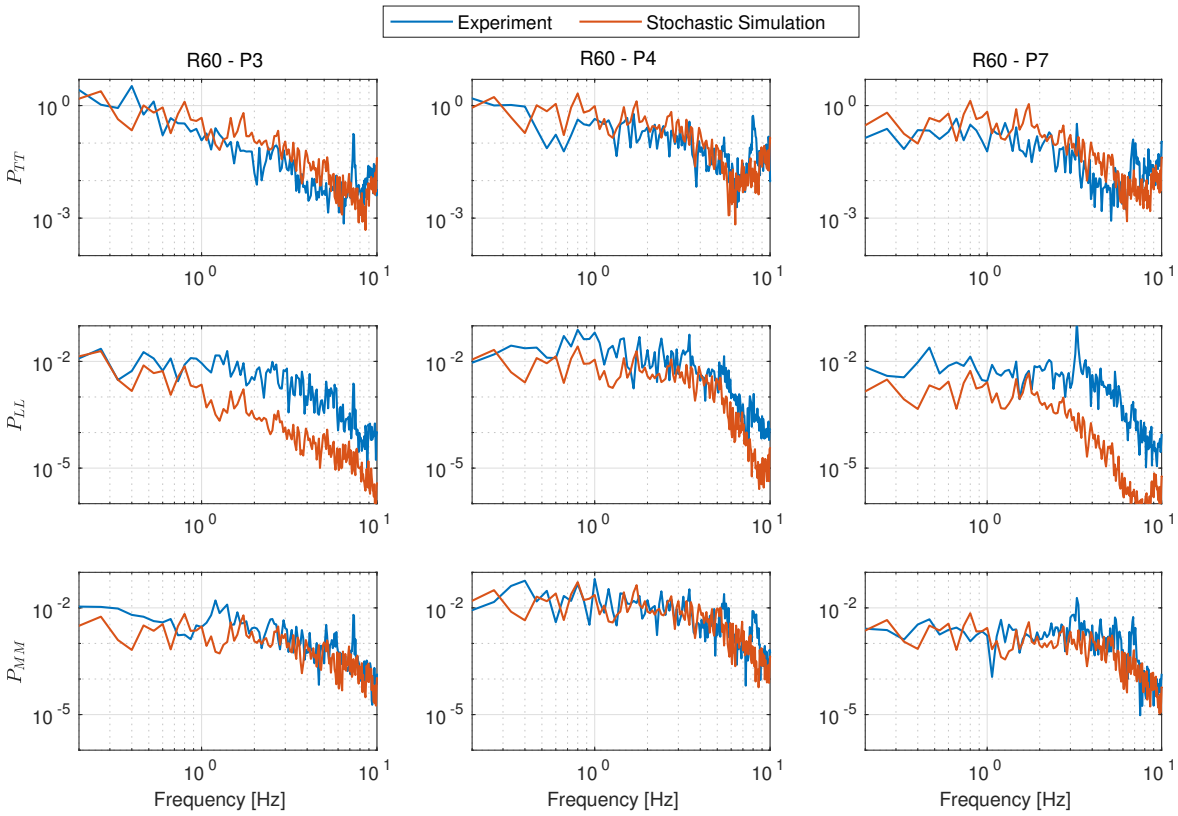

Fig. 8 PSD of the aerodynamic loads in R60 test condition.

headwind, R30 and R60. Among the experimental test points, three rotor positions were selected for the simulation at each wind direction. To represent the deterministic part of the airwake, the time-accurate CFD results were replaced by the time-averaged database, while the stochastic effects were generated through the output of AR filters. The time histories of the aerodynamic loads obtained during 30 seconds of the simulation, were analysed in the frequency domain and the PSDs were compared with the experimental spectra. This comparison demonstrated the capability of the stochastic simulation to predict the unsteady loads in various wind directions and rotor positions over the deck. The results showed that depending on the wind direction, either lateral or longitudinal perturbations can be set nearly independently from the other two components to reproduce the corresponding moment. Moreover, regarding the high sensitivity of the thrust unsteadiness to the vertical gust, the optimization procedure resulted in a better match for the thrust spectrum to minimize the total error of the estimation. Furthermore, the results of the filter design showed that a third-order Auto-Regressive model is suitable to regenerate the airwake spectra obtained from the optimization. To perform the HSDI simulation based on the proposed stochastic approach, only the filter coefficients need to be stored and updated by moving the rotor over the deck. Consequently, the computational cost required for implementing the turbulent CFD flowfield is significantly reduced.

The proposed approach can be effectively implemented in a full-scale model to perform HSDI real-time simulations

with the pilot–in–the–loop. The hovering task over the deck will be performed and the effect of the stochastic airwake on the low-frequency control activities and pilot workload will be assessed. Furthermore, the filters could be designed for an extended area over the deck, providing enough space to perform a dynamic test. Additionally, it has been shown in other test campaigns that it is possible to collect unsteady rotor loads during GVPM wind tunnel tests with a helicopter model moving along predefined flight trajectories. So, this may allow for the inclusion of the dynamics of the helicopter in the design of the turbulence shaping filters without applying any modification to the algorithm presented here. Ultimately, the presented approach based on a combination of wind tunnel experiments and numerical identification, may further enhance the possibility of developing more representative dynamic simulation models applicable in several WOD conditions to identify the boundaries of safe operation in ship helicopter operation, reducing significantly the number of required at sea flight tests.

References

[1] Healey, J. V., "The prospects for simulating the helicopter/ship interface," *Naval Engineers Journal*, Vol. 99, No. 2, 1987, pp. 45–63. https://doi.org/10.1111/j.1559-3584.1987.tb02099.x.

[2] Lumsden, R. B., Padfield, G. D., and Braby-Deighton, C. D., "Human Factors Challenges at the Helicopter-Ship Dynamic Interface," *SAE Technical Paper*, 1999. https://doi.org/10.4271/1999-01-5607.

[3] Hodge, S., Forrest, J., Padfield, G., and Owen, I., "Simulating the environment at the helicopter-ship dynamic interface: research, development and application," *Aeronautical Journal*, Vol. 116, No. 1185, 2012, p. 1155. https://doi.org/10.1017/S0001924000007545.

[4] Padfield, G. D., "Rotorcraft Virtual Engineering; Supporting Life-Cycle Engineering through Design and Development, Test and Certification and Operations," *The Aeronautical Journal*, Vol. 122, 2018, p. pp. 1475–1495. https://doi.org/10.1017/aer.2018.47.

[5] Wilkinson, C. H., Roscoe, M. F., and VanderVeliet, G. M., "Determining fidelity standards for the shipboard launch and recovery task," *AIAA Modeling and Simulation Technologies Conference and Exhibit*, 2001. https://doi.org/10.2514/6.2001-4062.

[6] Hodge, S. J., Zan, S. J., Roper, D. M., Padfield, G. D., and Owen, I., "Time-Accurate Ship Airwake and Unsteady Aerodynamic Loads Modeling for Maritime Helicopter Simulation," *Journal of the American Helicopter Society*, Vol. 54, No. 2, 2009, pp. 022005–1–16. https://doi.org/10.4050/JAHS.54.022005.

[7] Bunnell, J. W., "An integrated time varying airwake in a UH-60 black hawk shipboard landing simlation," *AIAA Modeling and Simulation Technologies Conference and Exhibit*, 2001. https://doi.org/10.2514/6.2001-4065.

[8] Roper, D. M., Owen, I., Padfield, G. D., and Hodge, S. J., "Integrating CFD and piloted simulation to quantify ship-helicopter operating limits," *The Aeronautical Journal*, Vol. 110, No. 1109, 2006, p. 419–428. https://doi.org/10.1017/S0001924000001329.

[9] Tan, J. F., Zhou, T. Y., Sun, Y. M., and Barakos, G. N., "Numerical investigation of the aerodynamic interaction between a tiltrotor and a tandem rotor during shipboard operations," *Aerospace Science and Technology*, Vol. 87, 2019, pp. 62–72. https://doi.org/10.1016/j.ast.2019.02.005.

[10] Oruc, I., Horn, J. F., Shipman, J., and Polsky, S., "Towards Real-Time Pilot-in-the-Loop CFD Simulations of Helicopter/Ship Dynamic Interface," *International Journal of Modeling, Simulation, and Scientific Computing*, Vol. 8, No. 4, 2017. https://doi.org/10.1142/S179396231743005X.

[11] Crozon, C., Steijl, R., and Barakos, G. N., "Coupled flight dynamics and CFD – demonstration for helicopters in shipborne environment," *The Aeronautical Journal*, Vol. 122, No. 1247, 2018, pp. 42–82. https://doi.org/10.1017/aer.2017.112.

[12] Oruc, I., and Horn, J. F., "Coupled Flight Dynamics and Computational Fluid Dynamics Simulations of Rotorcraft/Terrain Interactions," *Journal of Aircraft*, Vol. 54, No. 6, 2017, pp. 2228–2241. https://doi.org/10.2514/1.C034101.

[13] Lee, D., Sezer-Uzol, N., Horn, J. F., and Long, L. N., "Simulation of Helicopter Shipboard Launch and Recovery with Time-Accurate Airwakes," *Journal of Aircraft*, Vol. 42, No. 2, 2005, pp. 448–461. https://doi.org/10.2514/1.6786.

[14] Chirico, G., Szubert, D., Vigevano, L., and Barakos, G. N., "Numerical Modelling of the Aerodynamic Interference between Helicopter and Ground Obstacles," *CEAS Aeronautical Journal*, Vol. 8, No. 4, 2017, pp. 589–611. https://doi.org/10.1007/s13272-017-0259-y.

[15] Labows, S. J., and Tischler, M. B., "UH-60 Black Hawk Disturbance Rejection Study for Hover/Low Speed Handling Qualities Criteria and Turbulence Modeling," *American Helicopter Society 56th Annual Forum*, 2000.

[16] Lusardi, J. A., Tischler, M. B., Blanken, C. L., and Labows, S. J., "Empirically Derived Helicopter Response Model and Control System Requirements for Flight in Turbulence," *Journal of American Helicopter Society*, Vol. 49, No. 3, 2004, pp. 340–349. https://doi.org/10.4050/JAHS.49.340.

[17] McLean, D., *Automatic Flight Control Systems*, 1st ed., Prentice Hall International (UK) Ltd, Hertfordshire, 1990, Chap. 5, pp. 127–135.

[18] Lee, D., and Horn, J. F., "Analysis of Pilot Workload in the Helicopter/Ship Dynamic Interface Using Time-Accurate and Stochastic Ship Airwake Models," *AIAA Atmospheric Flight Mechanics Conference and Exhibit*, 2004. https://doi.org/10.2514/6.2004-5360.

[19] Lee, D., and Horn, J. F., "Simulation of pilot workload for a helicopter operating in a turbulent ship airwake," *Proceedings of the Institution of Mechanical Engineers, Part G: Journal of Aerospace Engineering*, Vol. 219, No. 5, 2005, pp. 445–458. https://doi.org/10.1243/095441005X30298.

[20] Padfield, G. D., *Helicopter flight dynamics: the theory and application of flying qualities and simulation modelling*, John Wiley & Sons, 2008.

[21] Ly, U.-L., and Chan, Y. K., "Time-Domain Computation of Aircraft Gust Covariance Matrices," *AIAA Atmospheric Flight Mechanics Conference and Exhibit*, 1980. https://doi.org/10.2514/6.1980-1615.

[22] Sparbanie, S. M., Horn, J. F., Geiger, D. H., and Sahasrabudhe, V., "A Stochastic Model of Unsteady Ship Airwake Disturbances on Rotorcraft," *American Helicopter Society 65th Annual Forum*, 2009.

[23] Horn, J. F., Sparbanie, S. M., Cooper, J., and Schierman, J., "On-Line Identification of Ship Airwake Disturbances on Rotorcraft," *American Helicopter Society 65th Annual Forum*, 2009.

[24] Gaonkar, G. H., "Toward a Complete Stochastic Model of Airwake Turbulence for Helicopter Shipboar Operations," *American Helicopter Society 63rd Annual Forum*, 2007.

[25] Gaonkar, G. H., and Mohan, R., "Extracting Stochastic Airwake Models from a Database for Engineering Analysis and Simulation," *Journal of the American Helicopter Society*, Vol. 57, No. 2, 2012, pp. 1–15. https://doi.org/10.4050/JAHS.57.022004.

[26] Hoblit, F. M., *Gust loads on aircraft: concepts and applications*, AIAA, 1988.

[27] Vitale, A., Corraro, G., Corraro, F., and Gallas, Q., "Ship Airwake Identification from Experimental Data for Automatic Deck Landing and Takeoff," *Journal of Aircraft*, 2022, pp. 1–11. https://doi.org/10.2514/1.C036887.

[28] Lee, R. G., and Zan, S. J., "Wind tunnel testing of a helicopter fuselage and rotor in a ship airwake," *Journal of the American Helicopter Society*, Vol. 49, No. 2, 2004, pp. 149–159. https://doi.org/10.4050/1.3092869.

[29] Taymourtash, N., Zagaglia, D., Zanotti, A., Muscarello, V., Gibertini, G., and Quaranta, G., "Experimental study of a helicopter model in shipboard operations," *Aerospace Science and Technology*, Vol. 61, 2021, pp. 97–108. https://doi.org/10.1016/j.ast.2021.106774.

[30] Taymourtash, N., Zanotti, A., Gibertini, G., and Quaranta, G., "Unsteady load assessment of a scaled-helicopter model in a ship airwake," *Aerospace Science and Technology*, Vol. 129, 2022. https://doi.org/10.1016/j.ast.2022.107583.

[31] Anon., "Aeronautical Design Standard Performance Specification Handling Qualities Requirements For Military Rotorcraft, ADS-33E-PRF," , 2000.

[32] Masarati, P., Morandini, M., and Mantegazza, P., "An efficient formulation for general-purpose multibody/multiphysics analysis," *ASME Journal of Computational Nonlinear Dynamics*, Vol. 9, No. 4, 2014, pp. 041001–041001–9. https://doi.org/10.1115/1.4025628.

[33] Masarati, P., Piatak, D. J., Quaranta, G., Singleton, J. D., and Shen, J., "Soft Inplane Tiltrotor Aeromechanics Investigation Using Two Comprehensive Multibody Solvers," *Journal of the American Helicopter Society*, Vol. 53, No. 2, 2008, pp. 179–192. https://doi.org/10.4050/JAHS.53.179.

[34] Ghiringhelli, G. L., Masarati, P., and Mantegazza, P., "Multibody Implementation of Finite Volume C Beams," *AIAA Journal*, Vol. 38, No. 1, 2000, pp. 131–138. https://doi.org/10.2514/2.933.

[35] Peters, D. A., Boyd, D. D., and He, C. J., "Finite-State Induced-Flow Model for Rotors in Hover and Forward Flight," *Journal of the American Helicopter Society*, Vol. 34, No. 4, 1989, pp. 5–17. https://doi.org/10.4050/JAHS.34.5.

[36] Toffoletto, R., Reddy, K., and Lewis, J., "Effect of ship frontal variation on the flow field in the flight-deck region," *Computational Fluid Dynamics 2002: Proceedings of the Second International Conference on Computational Fluid Dynamics, ICCFD, Sydney, Australia, 15–19 July 2002*, Springer, 2003, pp. 191–196. https://doi.org/10.1007/978-3-642-59334-5_26.

[37] Syms, G., "Simulation of simplified-frigate airwakes using a lattice-Boltzmann method," *Journal of Wind Engineering and Industrial Aerodynamics*, Vol. 96, No. 6-7, 2008, pp. 1197–1206. https://doi.org/10.1016/j.jweia.2007.06.040.

[38] Bardera-Mora, R., Conesa, A., and Lozano, I., "Simple frigate shape plasma flow control," *Proceedings of the Institution of Mechanical Engineers, Part G: Journal of Aerospace Engineering*, Vol. 230, No. 14, 2016, pp. 2693–2699. https://doi.org/10.1177/0954410016630333.

[39] Forrest, J. S., Hodge, S. J., Owen, I., and Padfield, G. D., "An investigation of ship airwake phenomena using time-accurate CFD and piloted helicopter flight simulation," *34th European Rotorcraft Forum*, 2008.

[40] Morelli, E. A., "Flight Test Maneuvers for Efficient Aerodynamic Modeling," *Journal of Aircraft*, Vol. 49, No. 6, 2012, pp. 1857–1867. https://doi.org/10.2514/1.C031699.

[41] Klein, V., and Morelli, E. A., *aircraft system identification – theory and practice*, AIAA Education Series, AIAA, Reston, VA, 2006.

[42] Schroeder, M., "Synthesis of low-peak-factor signals and binary sequences with low autocorrelation (Corresp.)," *IEEE Transactions on Information Theory*, Vol. 16, No. 1, 1970, pp. 85–89. https://doi.org/10.1109/TIT.1970.1054411.

[43] MATLAB, *version 9.9.0.1495850 (R2020b)*, The MathWorks Inc., Natick, Massachusetts, 2020.

[44] Rao, C., *Linear Statistical Inference and Its Applications*, Wiley, New York, NY, USA, 1965.

[45] Stoica, P., Babu, P., and Li, J., "New Method of Sparse Parameter Estimation in Separable Models and Its Use for Spectral Analysis of Irregularly Sampled Data," *IEEE Transactions on Signal Processing*, Vol. 59, No. 1, 2011, pp. 35–47. https://doi.org/10.1109/TSP.2010.2086452.